Available online at www.sciencedirect.com
ScienceDirect
Journal of Power Sources 166 (2007) 104–111
JOURNAL OF POWER SOURCES
www.elsevier.com/locate/jpowsour

Use of cellulose-based carbon aerogels as catalyst support for PEM fuel cell electrodes: Electrochemical characterization

Elodie Guilminot [a], Florent Fischer [b], Marian Chatenet [a,*], Arnaud Rigacci [b], Sandrine Berthon-Fabry [b], Patrick Achard [b], Eric Chainet [a]

[a] *Laboratoire d'Electrochimie et de Physicochimie des Matériaux et des Interfaces (LEPMI), UMR 5631 CNRS-INPG-UJF, 1130 rue de la Piscine, BP 75, 38402 Saint Martin d'Hères Cedex, France*
[b] *Ecole des Mines de Paris, Center for Energy and Processes (CEP), FRE CNRS 2861, rue Claude Daunesse, BP 207, 06904 Sophia Antipolis Cedex, France*

Received 5 July 2006; received in revised form 17 November 2006; accepted 28 December 2006
Available online 16 January 2007

Abstract

New nanostructured carbons have been developed through pyrolysis of organic aerogels, based on supercritical drying of cellulose acetate gels. These cellulose acetate-based carbon aerogels (CA) are activated by CO_2 at 800 °C and impregnated by $PtCl_6^{2-}$; the platinum salt is then chemically or electrochemically reduced. The resulting platinized carbon aerogels (Pt/CA) are characterized with transmission electron microscopy (TEM) and electrochemistry. The active area of platinum is estimated from hydrogen adsorption/desorption or CO-stripping voltammetry: it is possible to deposit platinum nanoparticles onto the cellulose acetate-based carbon aerogel surface in significant proportions. The oxygen reduction reaction (ORR) kinetic parameters of the Pt/CA materials, determined from quasi-steady-state voltammetry, are comparable with that of Pt/Vulcan XC72R. These cellulose acetate-based carbon aerogels are thus promising electrocatalyst support for PEM application.

Keywords: Cellulose acetate; Carbon aerogel; Electrocatalyst support; Platinum nanoparticles; PEM fuel cell

1. Introduction

The recent interest for clean energies gives rise to many studies on the Proton Exchange Membrane Fuel Cell (PEMFC). The PEMFC performances depend on various factors, among which are the nature, physicochemical properties and electrochemical activity of the electrode materials. The current PEMFC electrode materials consist of carbon black (e.g. Vulcan XC72) and noble electrocatalysts (e.g. platinum nanoparticles dispersed over high area carbon) [1]. Since 15 years, a new class of electrode materials has been evaluated as high area carbon substrate: carbon aerogel (CA). Aerogels are nanoporous and nanostructured materials produced via a sol–gel process followed by supercritical drying. Carbon aerogels are obtained from pyrolysis of organic aerogels. Carbon aerogels from the resorcinol–formaldehyde (RF) systems, first synthesized by Pekala, have both good electronic conductivities [2] and high surface areas, along with controllable porosity: it is possible to design CA with high mesoporous and low microporous volumes [3]. Such physical structures and physicochemical properties are adapted to electrochemical applications, like supercapacitors or fuel cell electrodes (upon doping by noble metal) [4,5]. Glora et al. recently considered their use in PEMFCs [6]; Pt-doped carbon aerogels (Pt/CA) may display better electrochemical activity than commercial or homemade Pt-doped carbon blacks [7]. An interesting feature of carbon aerogels is that their structural properties can be adapted almost on demand [8,9], so as to improve their applicability for fuel cell electrodes [10]. Consequently, several recent studies concern the tests of other carbon aerogel precursors for use as PEMFC materials [11,12]. Among these news materials, the Center for Energy and Processes of Ecole des Mines de Paris at Sophia Antipolis has elaborated *green* materials consisting of carbon aerogels resulting from the pyrolysis of cellulose acetate aerogels; they display a large surface area and an appropriate chemical/mechanical stability as reported by Jin et al. [13].

* Corresponding author. Tel.: +33 476 82 65 88; fax: +33 476 82 67 77.
E-mail address: Marian.Chatenet@lepmi.inpg.fr (M. Chatenet).

0378-7753/$ – see front matter © 2007 Elsevier B.V. All rights reserved.
doi:10.1016/j.jpowsour.2006.12.084

In this paper, we evaluate the capacity to use such cellulose acetate-based carbon aerogels as PEMFC electrode materials. The first step is to *dope* the various carbon aerogels by platinum nanoparticles. The active area of deposited platinum (S_{Pt}) is then determined from the coulometry of hydrogen-adsorption/desorption (S_{Pt-H}) and CO-stripping (S_{Pt-CO}). Second, the resulting Pt/CA were characterized in term of oxygen reduction reaction (ORR) electroactivity, using the classical rotating disk electrode (RDE) setup [14].

2. Experimental

2.1. Carbon aerogel synthesis

The sol–gel system is based on the crosslinking of cellulose acetate (Aldrich, Mn = 50,000) with polyfunctional isocyanate (MDI, functionality = 2.7) in acetone. The reaction is catalysed by dibutyltin dilaurate, using a mass ratio between catalyst and reagents of ca. 5%. The mass of cellulose acetate used was 10 times larger than that of isocyanate. The gelation time was ca. 30 min. During the syneresis stage, the gel was washed three times with pure acetone and aged for 7 days at room temperature. It was then dried in supercritical CO_2 conditions (80 bars, 40 °C) [15], after which it underwent pyrolysis in flowing nitrogen, as thoroughly described in Ref. [16].

Such cellulose acetate-based carbon aerogels display nanoscale structuration, high specific surface area and low density ca. 0.16 g cm^{-3}.

2.2. Carbon aerogel activation

The CA was first finely grounded. The grounded CA was then activated in CO_2 atmosphere at 800 °C during 1 h and gently cooled down to ambient temperature in 1 h under a CO_2 stream. The BET surface area was calculated from N_2 adsorption isotherm over the relative pressure (P/P_0) range of ca. 0.09–0.25. The activated or *raw* (not activated) CA chemical surface groups were investigated by Fourier Transformed Infrared (FTIR) spectroscopy before platinum insertion. For that purpose, we mixed 1 mg CA powder with 500 mg of KBr in an agate mortar; the resulting mixture was pressed successively at 5 tonnes for 3 min and at 10 tonnes for 3 min, so as to obtain a pellet. The FTIR spectra were recorded on a Nicolet 710 spectrometer between 4000 and 225 cm^{-1} with 100 scans at 4 cm^{-1} resolution.

2.3. Platinum salt insertion and reduction

The impregnation step was done immediately after activation, suspending 50 mg grounded CA powder for 24–48 h in 3 mL water–isopropanol (1:1) solution containing H_2PtCl_6 (0.017 M) under constant magnetic stirring. After impregnation, the platinum salt was reduced either electrochemically or chemically. The targeted platinum loading was 20 wt% Pt/CA: $m_{Pt}/(m_{Pt} + m_{CA}) = 0.2$.

The electrochemical reduction was performed before the electrochemical measurements by a series of intensiostatic pulses directly in the electrochemical characterization cell (1 M H_2SO_4) according to a procedure similar to that thoroughly described in Ref. [17]. We applied 1 prepulse at $I = -0.1$ A for 0.1 s so as to nucleate metallic platinum clusters, then 8 pulses at $I = -0.01$ A for 1 s to grow the platinum nanoparticles [18]. Between each pulse, the system is at open-circuit potential during 60 s to homogenize the solution (by diffusion) and evacuate the possible hydrogen bubbles (produced at low potentials during the cathodic pulse) [17,18].

The chemical reduction was done with an excess amount of $NaBH_4$ (×4) directly poured in the impregnation solution, in an ultrasonic bath. The CA was then washed with 500 mL boiling water and filtered, to remove the unreduced platinum salt and boron-containing species (mainly boric acid [7]), and dried by evaporation at 50 °C.

2.4. Electrochemical characterization

To study the CA electrochemical activity, an active layer was prepared from a suspension blend: 10 mg of CA was mixed with 200 mg of 5 wt% Nafion® solution (Aldrich), 600 μL of ultra-pure water and 300 μL of isopropanol. A 10 μL drop of this suspension was deposited on a glassy-carbon electrode (area = 0.196 cm^2) previously polished with diamond paste (down to 1 μm), and washed for 15 min in two successive ultrasonic baths of acetone and ultra-pure water. The resulting layer (containing ca. 91 μg Pt/CA that is 18 μg Pt) was dried for 12 h and then heated for 15 min at 150 °C to reconstitute Nafion®. We point out these new materials display complex surface chemistry, which is still very badly known, inducing non-negligible uncertainties in platinum loadings. We nevertheless considered that the whole targeted Pt was indeed present onto the CA after impregnation/reduction of the $PtCl_6^{2-}$ salt; we used the targeted Pt loading for the mass activity (MA) calculations.

The experiments were carried out on a rotating disk electrode (EDT 101, Tacussel) setup in 1 M sulphuric acid (Suprapur Merck) at room temperature (20 ± 3 °C). The electrochemical cell was connected to a potentiostat PAR 273 (EG&G) with a Pt counter electrode and a saturated calomel electrode (SCE, +0.245 V versus RHE) as reference. All the potentials are nevertheless expressed on the reference hydrogen electrode (RHE) scale.

The active area of platinum was determined from hydrogen-desorption coulometry: the cell was deaerated by inert gas (N_2 N45, Messer) bubbling in the solution for 15 min; during the measurements, the nitrogen stream was held above the solution. Two CV cycles were then monitored at 10 mV s^{-1} from 45 to 1445 mV versus RHE: the active area of platinum was calculated from hydrogen-desorption coulometry in the second cycle (the charge related to this reaction is 210 μC cm^{-2}). The uncertainties presented in Table 1 result from the reproducibility measurements attempted on several identical experiments (typically more than 3).

For CO-stripping coulometry, the solution was first saturated with carbon monoxide following 3–5 min of CO (N45, Alphagaz) bubbling, and second deaerated by inert gas (N_2) bubbling in the solution for 15 min to remove any trace of bulk CO in the electrolyte. During these 18–20 min, the electrode was

Table 1
Influence of the CA pyrolysis temperature on the Pt active area determined from H-desorption or CO-stripping coulometries, for the Pt/CA samples; chemical or (*) electrochemical reduction of $PtCl_6^{2-}$

Pt/CA samples	S_{Pt-H} (hydrogen-desorption coulometry) (cm^2)	S_{Pt-CO} (CO-stripping coulometry) (cm^2)
$T_{pyrolysis} = 550\,^{\circ}C$	0.5 ± 0.2	1.4 ± 0.4
$T_{pyrolysis} = 750\,^{\circ}C$	1.6 ± 0.3 2.3 ± 0.3 (*)	5.3 ± 0.8 3.8 ± 0.5 (*)
$T_{pyrolysis} = 950\,^{\circ}C$	2.1 ± 0.3	2 ± 0.4

held at 45 mV versus RHE. Then two CV cycles were recorded at 50 mV s^{-1} from 45 to 1445 mV versus RHE, an inert gas stream being held above the solution. The active area of platinum was then determined from the CO-stripping peak coulometry (in the potential range from around 600 to 1200 mV versus RHE), assuming a full monolayer of CO was adsorbed over platinum, which corresponds to 420 μC cm^{-2}.

ORR kinetics parameters determination was undertaken for oxygen-saturated electrolytes, a permanent O_2 bubbling being maintained during the measurements to prevent any O_2 depletion in the electrolyte. Before the voltammetry, the working electrode was held for 1 min at 945 mV versus RHE to ensure a reproducible platinum state of surface. The quasi-steady-state voltammograms were recorded at 1 mV s^{-1} from 945 to 145 mV versus RHE varying the RDE rotation speed from 500 to 4000 rpm.

3. Results and discussion

3.1. Influence of the carbon aerogel surface groups for platinum insertion

The carbon aerogel activation (1 h heating at 800 °C in CO_2 atmosphere, followed by cooling down under CO_2 atmosphere) yields 17–20% burn-off, while the CA surface area increases from 400 to 450 $m^2\,g^{-1}$ (as measured from nitrogen-sorption measurements, not shown). As a result, the CO_2 activation modifies the carbon porosity: it indeed produces an opening, followed by the widening of the narrow microporosity, as already discussed by Rodriguez-Reinoso et al. [19]. The microporosity creation may also compete with microporosity widening up to the range of mesoporosity [20]. In our application (PEMFC electrodes), the mesoporosity is crucial, since it enables the reactants to access the active sites (platinum nanoparticles) and the penetration of Nafion® during the electrode elaboration [8,9]. The microporosity widening is especially noticeable at high burn-off rates (40–50%) [19,21]. However, burn-off above 50–60% may destruct the internal CA structure, inducing porosity decrease; such process is more severe at higher activation temperature, typically above ca. 900 °C [20].

The surface area after activation: ca. 450 $m^2\,g^{-1}$ as determined from N_2-sorption measurement is appropriate for use in PEMFC active layers. It is a compromise between: (i) high BET area, enabling better dispersion of the platinum nanoparticles over the CA substrate and (ii) important mesoporosity

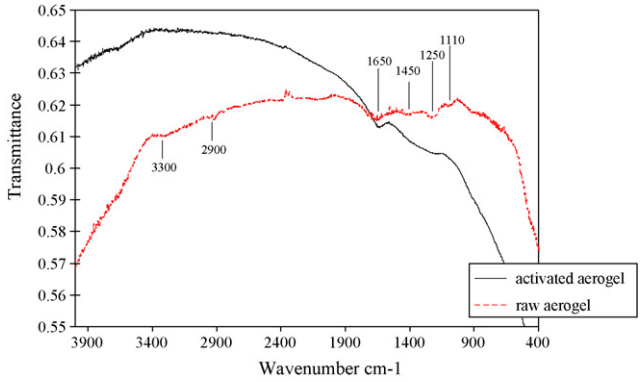

Fig. 1. FTIR spectra for activated and raw CA.

enabling good electrocatalyst utilization [7,9]. However, it is probably still possible to improve the micro/mesoporosity ratio by modifying the CA synthesis or activation procedures.

The thermal activation also modifies the CA surface chemistry, as shown on the FTIR spectra of Fig. 1 for raw or activated CA (free of any platinum). Let we first point out that the baseline drifts may follow the possible heterogeneity of our samples. Inspite of the uncertainties, these spectra clearly show an evolution of the CA surface chemistry.

Many bands are monitored for the raw carbon aerogel, displaying its important coverage by oxide groups: (i) the band at about 3300 cm^{-1} can be ascribed to ν(O–H) vibrations in hydroxyl groups, (ii) at 2900 cm^{-1} we monitor the vibrations ν_{as}(C–H) and ν_s(C–H) of methyl and methylene groups, (iii) organic compounds can also be detected: the δ_{as}(C–H) vibration is located at around 1450 cm^{-1} [22–25], (iv) the band at 1250 cm^{-1} can be attributed to ν(C–O): it may be connected with ethers (–OCH_3), or esters (CH_3–CO–O), or even acyclic C–O–C group [22,24], (v) the band at 1110 cm^{-1} is caused by ν(C–O) vibrations in secondary C–OH and finally (vi) the identification of the band at 1650 cm^{-1} varies in the literature: it could result from the ν(C=C) vibrations [22,23], but Lua and Guo [24] associate it to the ν(C=O) vibrations in quinones (graphite can display absorption bands in the ν(C=O) and the aromatic ν(C=C) vibrations regions [22,25]).

During the activation procedure, CO_2 oxidizes carbon into CO; the oxygenated, ether and ketone groups, are likely thermally unstable and may transform rapidly [23] (at high temperatures, e.g. activation above 700 °C, oxygen complexes (e.g. phenolic groups) are thermally unstable and hence decompose [23,24]). Indeed, most of the surface aromatic C=C bonds and oxygen groups (hydroxyl, methyl and methylene groups), typical of lignocellulosic materials [22], are eliminated after CO_2 activation at 800 °C: only the band at 1650 cm^{-1} remains significant after activation and its intensity increases. So, the activation probably favours the formation of C=O, typical of quinone groups, as confirmed by electrochemistry (see further). These results are in line with Lua and Guo conclusions [24]. The cellulose acetate-based CA complex surface chemistry (after pyrolysis) thus changes greatly upon activation. Such *cleaning* of the CA surface facilitates the anionic platinum adsorption from chloroplatinic acid impregnation, which is known to be favoured

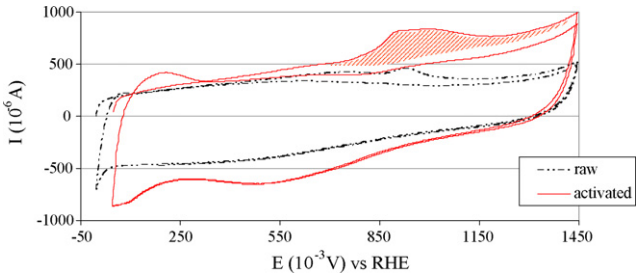

Fig. 2. Influence of the activation on the CO-stripping voltammograms for Pt/raw CA and Pt/activated CA (electrochemical reduction)—1 M sulphuric acid solution at 20 °C; 50 mV s^{-1}.

for carbon substrates free of oxygenated surface groups [26–28]. So, the CO_2 activation process renders the carbon surface more stable from a chemical point of view.

After platinum insertion, these activated or raw cellulose acetate-based CA are characterized electrochemically by CO-stripping (Fig. 2). The voltammogram for activated CA displays higher double layer currents than for raw CA. The resulting double layer capacities, ca. 6000 and 6800 μF for the raw and activated CA, respectively, correlate well with the porosity [29] (the same amount of CA powder was immobilized on the RDE tip in all experiments). Using the well admitted value for Vulcan XC72: $C_{dl} = 10\ \mu F\ cm^{-2}$ [30], and knowing that the voltammograms are obtained with ca. 0.09 mg carbon, the surface area is estimated at ca. 660 or 750 $m^2\ g^{-1}$ for the raw or activated CA, respectively. After platinum impregnation and reduction (especially chemical reduction, see Section 3.3), the CA electrochemical surface areas are higher than the BET surface areas measured before platinum insertion procedure (around 400 and 450 $m^2\ g^{-1}$ for raw and activated CA, respectively). This can result from double layer current over-estimation, probably following the inappropriate reference C_{dl} value taken from Vulcan XC72. We also point out that such very high surface area for the CA renders complex the active area of platinum determination either from CO-stripping or H-desorption coulometry (see below). However, the electrochemical results confirm those from BET measurements: the activation yields increased surface area, particularly due to higher mesoporosity (which is detected electrochemically).

The platinum active area can be determined from CO-stripping coulometry ($S_{Pt–CO}$, hatched surface in Fig. 2), after subtracting the double layer current (from the second CV cycle, in the absence of CO) corrected from the current offset. This current offset varies between 55 and 155 μA; it probably corresponds to the carbon superficial oxidation (quinone groups mainly, see above). During the CO bubbling at 45 mV versus RHE, the very reducing conditions can partly reduce some of these quinone groups from the CA surface, yielding hydroquinone species. Thus, the current gradual increase in the first cycle would be associated both to the CO-stripping and to the oxidation of hydroquinone into quinone. As the carbon is no longer in reducing medium during the cathodic scan (all traces of CO in solution have been purged; the electrode is not maintained at low potentials), the quinone groups are stable after their re-formation, and the double layer current (relative to carbon surface groups) does not vary anymore in the second cycle. Inspite of this correction, the integration under the peak must be done up to high potential (1400 mV versus RHE), which probably induces slight over-estimation of the platinum active area. The uncertainties of this method are about 15 to 30%, resulting from: (i) the very large CA double layer current inducing errors in the subtraction and (ii) the uncertainty in the current offset determination. The active area of platinum is ca. $S_{Pt–CO} = 3.8 \pm 0.5\ m^2\ g^{-1}$ for the activated CA (electrochemical reduction), while it is only ca. $S_{Pt–CO} = 1.5 \pm 0.5\ m^2\ g^{-1}$ for the raw CA. The CO_2 activation increases by a factor 2 the active area of platinum on the CA. As these values were calculated using the same amount of CA powder, it confirms the interest of the oxygenated groups removal from the carbon surface during the activation. Such improvement can be linked to: (i) the increase of CA surface area (evidence by the larger double layer currents for activated CA), yielding better platinum salt dispersion upon impregnation and (ii) the modification of the CA surface chemistry: carbon surface free from oxide groups (for activated CA) is available for $PtCl_6^{2-}$ adsorption in the impregnation step [26–28]. Moreover, the presence of mild acidic groups like quinone is favourable: it enhances the platinum dispersion over the carbon substrate [26], and thus reinforces the benefit of our thermal activation procedure.

In addition to the platinum specific area (amount deposited) differences, the shape and the potential of the CO-stripping peak varies. The CO-stripping peak for activated CA spreads up to high potentials, which can be linked to a wider platinum nanoparticles size distribution than in the case of the raw CA (lower potential corresponds to large Pt particles [31]). The activated CA probably also contains smaller Pt particles than the raw CA, which agrees with the interest of having a *clean* carbon surface for the platinum impregnation step.

3.2. Influence of the chemical or electrochemical reduction

After impregnation with $PtCl_6^{2-}$ salt, the Pt^{z+} species can be chemically or electrochemically reduced. We compared the materials resulting from these two reducing procedure following S_{Pt} determination from hydrogen-adsorption/desorption (Fig. 3a) or CO-stripping voltammetry (Fig. 3b). The voltammograms display large differences of double layer currents. For the chemical reduction, the double layer current is ca. 150 ± 60 μA (at 10 mV s^{-1} in Fig. 3a), whereas it is ca. 75 ± 30 μA for the electrochemical reduction. The same factor 2 exists with the curves in Fig. 3b at 50 mV s^{-1}. Part of the difference between the double layer currents can be allotted to the uncertainty on the quantity of deposited matter (including the experimental reproducibility issues). But such experimental error is not sufficient to explain the factor 2; so, we cannot rule out such double layer current evolution follows CA porosity modifications according to the platinum salt reduction procedure. Indeed, the strong reducing agent ($NaBH_4$) used in the chemical reduction, is likely to react with the CA surface groups (mainly quinone, see above), yielding increased porosity (oxides may obstruct micropores), or modify the graphitized areas of the sample (the disorder increases with $NaBH_4$ treatment) [32]. As a result, the

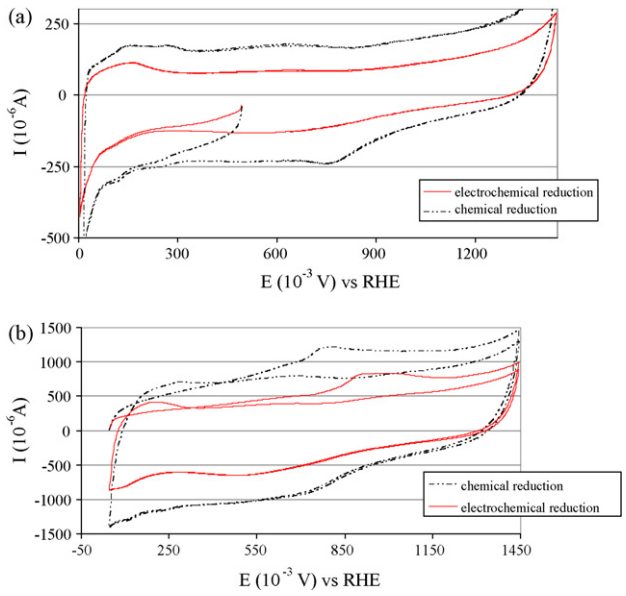

Fig. 3. Influence of $PtCl_6^{2-}$ reduction on H-adsorption/desorption voltammogram at 10 mV s^{-1} (a) or on CO-stripping voltammograms at 50 mV s^{-1} (b) for Pt/activated CA—1 M sulphuric acid solution at 20 °C.

microporosity may open upon contact with $NaBH_4$, yielding mesoporosity [33], as evidenced by the larger double layer currents on Fig. 3a. So in our case, we think contact of the CA with $NaBH_4$ did not remove all the CA surface oxygen groups (the quinone/hydroquinone peaks are still evidenced from 590 to 910 mV versus RHE), but nevertheless increased the CA active area (double layer capacity).

The platinum specific area calculated from hydrogen-desorption coulometry (Fig. 3a) is higher for the electrochemical reduction: $S_{Pt-H} = 2.3\,cm^2$ for the RDE active layer (corresponding to $13\,m^2\,g^{-1}$ Pt) than for the chemical reduction: $S_{Pt-H} = 1.6\,cm^2$ (i.e. $8.8\,m^2\,g^{-1}$ Pt) (Table 1, $T_{pyrolysis} = 750\,°C$). The values measured from CO-stripping (Fig. 3b) do not confirm such tendency and are higher overall: $S_{Pt-CO} = 5.3\,cm^2$ ($29\,m^2\,g^{-1}$ Pt) (chemical reduction) and $S_{Pt-CO} = 3.8\,cm^2$ ($21\,m^2\,g^{-1}$ Pt) (electrochemical reduction). As CO is one of the strongest poisons adsorbed on platinum, most pollutants originally adsorbed on the platinum should be displaced by its adsorption. Thus, the difference between S_{Pt-H} and S_{Pt-CO} can follow the presence of poisons [7]. The Pt/CA from chemical reduction is then probably more polluted than the Pt/CA from electrochemical reduction. The reason is likely: (i) the material *ageing* after activation with the chemical reduction, but even more (ii) the pollution from $NaBH_4$ oxidation products (mainly boric acid), which may obstruct the CA pores and strongly adsorb over Pt [7].

The CO-stripping peak potential (Fig. 3b) is lower for the chemical (800 mV versus RHE) than for the electrochemical reduction (925–1020 mV versus RHE). Assuming the conclusions from Maillard et al. [31], the chemical reduction would produce larger Pt particles (and agglomerates) than the electrochemical reduction. Moreover, as the CO-stripping peak spreads out more with the electrochemical reduction than with the chemical reduction, the Pt particles size dispersion is probably wider with electrochemical reduction, in agreement with the TEM characterization (Figs. 4 and 5).

Whatever the Pt salt reduction, the particles are heterogeneously distributed over the CA substrate and some carbon grains with no platinum particles are observed. When $PtCl_6^{2-}$ is electrochemically reduced (Fig. 4a), most of the Pt particles are small (2–5 nm), as revealed on the particle size distribution of Fig. 5a (calculated from 170 particles). Clusters (size > 15 nm) are also evidenced in a lower number but they represent 65% of the platinum specific surface (Fig. 5b). Anyway, the electrochemical reduction yields stable electrocatalysts particles [34], the size of which (mainly in the range 2–5 nm) is particularly adapted to the PEM application. However, the electrochemical reduction is hardly usable in an industrial process, conversely to the chemical reduction.

When $PtCl_6^{2-}$ is chemically reduced (Fig. 4b), all the platinum particles are organised in clusters. As a result, no accurate particle-size distribution can be determined. We think the strong

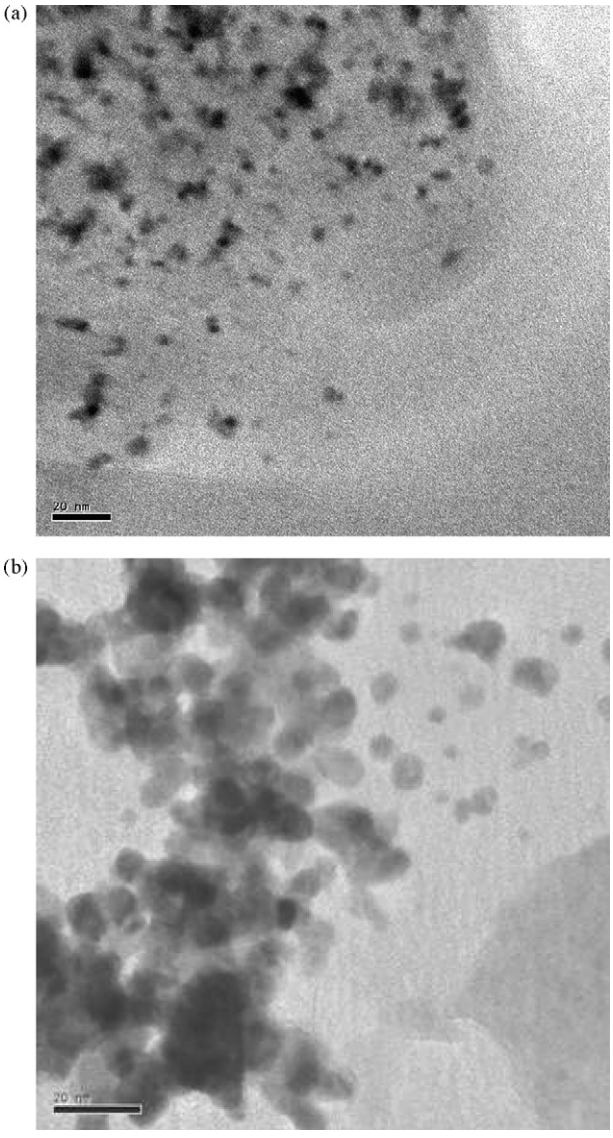

Fig. 4. Transmission electron micrographs for Pt/activated CA: electrochemical (a) or chemical (b) reduction.

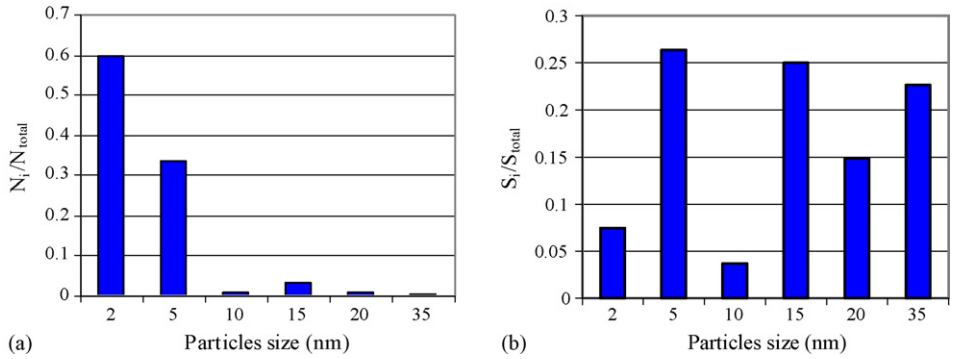

Fig. 5. Particles size distribution for Pt/activated CA (electrochemical reduction) according to their number (a) or their surface (b).

reducing agent (BH_4^-) modifies the carbon surface and changes the number (and the nature) of platinum adsorption sites: there might be platinum salt mobility on the carbon surface free from oxide groups, the diffusion of which directs platinum ions towards the already existing Pt (metal) nuclei (probably formed in areas easily accessed by BH_4^- species), forming bigger nanoparticles and agglomerates. However, the chemical reduction has the advantage of yielding higher platinum electrocatalytic activity, which is consistent with the higher particle (cluster) size, following the detrimental particle size effect for the ORR [35].

Despite these uncertainties, the following experiments are undertaken after chemical reduction of the $PtCl_6^{2-}$ species.

3.3. Influence of the CA pyrolysis temperature

The cellulose acetate-based aerogel has been pyrolyzed at 550, 750 or 950 °C. However, only the sample pyrolyzed at 750 °C has been synthesized in sufficient quantity to enable the optimization of the platinum insertion (which is material consuming). For the two other pyrolysis temperatures (550 and 950 °C), the electrochemical measurements are realized in the same experimental conditions than for the CA pyrolyzed at 750 °C.

The CO-stripping voltammograms from Fig. 6 show that I_{dl} varies from 700 μA for the CA pyrolyzed at 750 °C to ca. 150 μA for the other CA samples. Lower double layer currents likely result from smaller CA porosity, which is known to depend on the pyrolysis temperature [20,36]. For resorcinol/formaldehyde CA, the maximum porosity is obtained at ca. 900 °C, while for poly(vinylchloride) CA it is reached at ca. 550 °C. Now, high

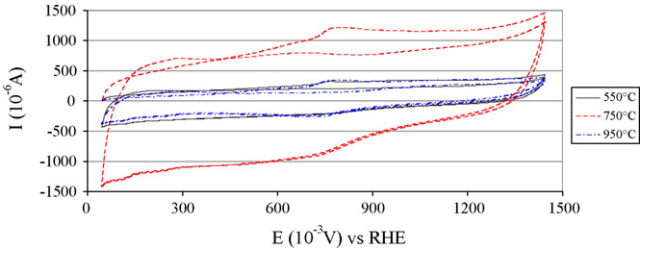

Fig. 6. Influence of the pyrolysis temperature on CO-stripping voltammograms Pt/activated CA—1 M sulphuric acid solution at 20 °C; 50 mV s^{-1}.

pyrolysis temperature may induce shrinkage of the carbon structure, resulting in lower porosity, as described by Ahmadpour and Do [20]. So, 950 °C might be too high of a pyrolysis temperature, resulting in lower CA porosity than at 750 °C. Conversely, the pyrolysis temperature of 550 °C remains much lower than the activation temperature (800 °C, optimized for the CA pyrolyzed at 750 °C): as a result, the activation may induce a densification of the CA structure, through a secondary carbonization process and thus decrease the CA surface area [20]. So neither the lowest (550 °C) nor highest (950 °C) pyrolysis temperatures yield satisfactory CA porosity. These results tend to show that: (i) the pyrolysis temperature has a great impact on the CA morphology but also (ii) the CA activation temperature must be chosen in agreement with the pyrolysis temperature.

The platinum specific area value is higher for the CA pyrolyzed at 750 °C (Table 1) but we cannot link for sure such better behaviour to the carbon aerogel physicochemical properties rather than to the optimization of the experimental conditions. However, the platinum specific area values evolve differently if they are determined by CO-stripping coulometry ($S_{Pt–CO}$) or by hydrogen desorption coulometry ($S_{Pt–H}$) (Table 1). The ratio $S_{Pt–H}/S_{Pt–CO}$ (which give an indication of the material cleanness [7]) is ca. 0.35, 0.30 and 1 for pyrolysis temperatures of 550 °C, 750 °C and 950 °C, respectively. High pyrolysis temperature yield lower pollution of the CA and higher platinum electrochemically active area. For low pyrolysis temperature (550 and 750 °C), the ratio is rather unchanged and consistent with non-negligible pollution of the CA. Thus, the pyrolysis temperature greatly influences the cleanness and the surface composition of the resulting CA, higher pyrolysis temperature yielding cleaner samples.

Finally, the potential and the shape of the CO-stripping peak do not change with the pyrolysis temperature (Fig. 6), showing that it does not dramatically influence the Pt particles size (the activation step has a greater influence, see Section 3.1) [31].

3.4. Oxygen reduction reaction kinetics parameters for Pt/CA

The performances of hydrogen-fed PEMFCs are not limited by the anodic reaction, which is fast (rate control from hydrogen mass transport to platinum nanoparticles [37]). Conversely, the cathode reaction (oxygen reduction reaction, ORR) is slow.

Table 2
Kinetics parameters (Tafel slopes (b) and current densities measured at 895 mV vs. RHE) for Pt/CA and commercial Pt/Vulcan XC72R nanoparticles

Materials	b (mV dec^{-1})	i_{895} (μA cm^{-2} geo)	MA_{895}[a] (A g^{-1} Pt)	SA_{895} (μA cm^{-2} Pt)
Pt/activated CA ($T_{pyrolysis}$ = 550 °C)	−86	−180	−2.0	−40
Pt/raw CA ($T_{pyrolysis}$ = 750 °C)	−101	−30	−0.33	−4.5
Pt/activated CA ($T_{pyrolysis}$ = 750 °C)	−89	−330	−3.6	−17.5
Pt/activated CA ($T_{pyrolysis}$ = 950 °C)	−93	−200	−2.2	−25
Vulcan XC72R + 20 wt% Pt	−77	50	−0.54	−25

[a] MA_{895} values calculated on the basis on the Pt loading predicted from the Pt/CA elaboration procedure (ca. 20 wt%).

Thus, we decided to benchmark our Pt/CA materials electrocatalytic activity towards the ORR.

The ORR kinetics parameters are determined from quasi-steady-state voltammograms (Fig. 7a). The calculation of i_k, the current density corrected from the oxygen diffusion in the solution, using $i_k = (i \times i_l)/(i_l - i)$ with i_l the limiting current, yields classical Tafel lines in the low current density region (Fig. 7b), from which we extract the Tafel slope (b) and the current density measured at 895 mV versus RHE (i_{895}), itself allowing to calculate the mass (MA_{895}) or specific (SA_{895}) ORR activities. These values (see Table 2) characterize the electrocatalytic activity of our Pt/CA nanoparticles [7,38]. For the benchmark catalysts (Pt/Vulcan XC72R), we find $b = -77$ mV dec^{-1}. Such value corresponds to a classical mechanism involving four electrons per oxygen molecule [38]. For Pt/activated CA, the Tafel slope is slightly lower, around −90 mV dec^{-1}. A ORR Tafel slope increase (in absolute value) in the range from ca. −60 to ca. −120 mV dec^{-1} was attributed to the decrease in platinum particles size (in alkaline medium) [17], and explained by the increase of the carbon support contribution towards the ORR [7].

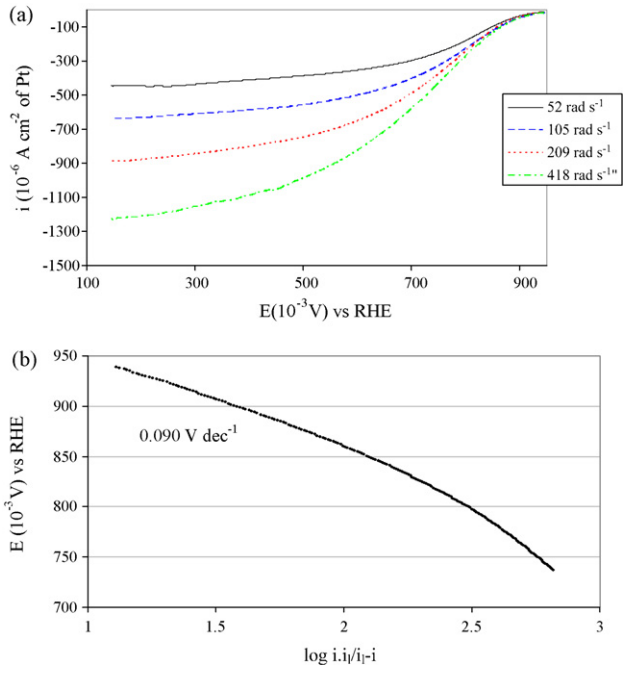

Fig. 7. Oxygen reduction reaction (ORR) experiments for Pt/activated CA–1 M sulphuric acid solution at 20 °C: (a) quasi-steady state voltammograms recorded at 1 mV s^{-1} and (b) Tafel slopes for geometric current densities corrected from the oxygen diffusion in the solution.

So, the carbon contribution of the CA substrate might be much higher than for Vulcan XC72; such findings agree with the CA large BET area (see above) and Marie et al. conclusions [7]: the larger the carbon surface area, the larger the Tafel slope. However, the lowest Tafel slope value (−101 mV dec^{-1}, Table 2) is measured with the raw CA, despite its smaller surface area than for the activated CA. This apparent contradiction probably results from the fact that raw CAs display more surface oxides (see Fig. 1), which increase the ORR rate on carbon (2-electron process) and promote the H_2O_2 dissociation [30].

SA_{895} values are smaller for Pt/CA pyrolyzed at 750 °C (−17.5 μA cm^{-2} Pt) than with Pt/Vulcan XC72 (−25 μA cm^{-2} Pt) (Table 2). We do not discuss the other Pt/CA samples, for which the lower Pt areas explain the (artificially) better SA values. On the other hand, MA_{895} (except for the raw CA) or the geometric current density is always higher with Pt/activated CA (−180, −330 and −200 μA cm^{-2} for $T_{pyrolysis}$ = 550, 750 and 950 °C, respectively) than for Pt/Vulcan XC72 (−50 μA cm^{-2}). Thus, the (positive) contribution of the carbon substrate in the ORR kinetic parameters is higher for Pt/activated CA than for Pt/Vulcan. This goes in line with the larger BET (or electrochemical: double layer) carbon area values we monitored (Fig. 2). These interesting results of ORR kinetic parameters on Pt/CA nanoparticles (which can still be improved) make the cellulose acetate-based carbon aerogels promising materials for PEM applications.

4. Conclusions

Carbon aerogels elaborated from a cellulose acetate precursor display high specific areas (above 400 m^2 g^{-1}), compatible with use as substrate for PEMFC electrocatalyst deposition. These specific areas can be increased by thermal activation treatment in CO_2 atmosphere, which yields chemically stable carbon surface, by eliminating most of the OH, CH_2, CH_3 and unstable CO groups. The raw CA surface chemistry is complex and the material remains heterogeneous even after activation. A better knowledge of the physicochemical surface properties would allow optimizing the Pt/CA synthesis especially regarding the quantity of platinum nanoparticles (diameter in the range 2–5 nm). Moreover, the platinum precursor impregnation and chemical reduction can modify the CA physicochemical properties. The pyrolysis temperature also influences the electrochemical properties of the cellulose acetate-based CA: the lower the temperature, the higher the aerogel pollution, yielding lower electrochemically active platinum area. The first

electrochemical results obtained with the Pt/CA samples are nevertheless promising: the amount of platinum deposited onto the CA is significant although the experimental conditions still need improvement. The ORR specific activities of the Pt/CA nanoparticles are comparable with that of the Pt/Vulcan XC72 benchmark, while their mass activities are slightly higher. In conclusion, these cellulose acetate-based CA show a good potential as electrocatalyst support for PEMFC applications; the study deserves to optimize their formulation (so as to target the appropriate physicochemical properties) and the protocol of platinum insertion.

Acknowledgements

The authors thank the European Commission for financial support (European project FP6 AEROCELL). They also gratefully acknowledge Bernard Simon (SAFT) for the BET measurements.

References

[1] W. Vielstich, A. Lamm, H. Gasteiger (Eds.), Handbook of Fuel Cells: Fundamentals, Technology, Applications, Wiley, New York, 2003.
[2] X. Lu, O. Nilsson, J. Fricke, R. Pekala, J. Appl. Phys. 73 (1993) 581.
[3] H. Tamon, H. Ishizaka, M. Mikami, M. Okazaki, Carbon 35 (1997) 791.
[4] R. Pekala, J. Farmer, C. Alviso, T. Tran, S. Mayer, J. Miller, B. Dunn, J. Non-Cryst. Solids 225 (1998) 74.
[5] C. Moreno-Castilla, F.J. Maldonado-Hodar, Carbon 43 (2005) 455.
[6] M. Glora, M. Wiener, R. Petricevic, H. Pröbstle, J. Fricke, J. Non-Cryst. Solids 285 (2001) 283.
[7] J. Marie, S. Berthon-Fabry, P. Achard, M. Chatenet, A. Pradourat, E. Chainet, J. Non-Cryst. Solids 350 (2004) 88.
[8] J. Marie, S. Berthon-Fabry, P. Achard, M. Chatenet, E. Chainet, R. Pirard, N. Cornet, ECS Trans. 1 (2006) 509.
[9] J. Marie, S. Berthon-Fabry, M. Chatenet, E. Chainet, N. Cornet, P. Achard, J. Appl. Electrochem. 37 (2007) 147.
[10] R. Petricevic, M. Glora, J. Fricke, Carbon 39 (2001) 857.
[11] A. Smirnova, X. Dong, H. Hara, A. Vasiliev, N. Sammes, Int. J. Hydrogen Energy 30 (2005) 149.
[12] W. Baker, J. Long, R. Stroud, D. Rolison, J. Non-Cryst. Solids 350 (2004) 80.
[13] H. Jin, Y. Nishiyama, M. Wada, S. Kuga, Colloids Surf. A: Physicochem. Eng. Aspects 240 (2004) 63.
[14] F. Gloaguen, F. Andolfatto, R. Durand, P. Ozil, J. Appl. Electrochem. 24 (1994) 863.
[15] F. Fischer, A. Rigacci, R. Pirard, S. Berthon-Fabry, P. Achard, Polymer 47 (2006) 7636.
[16] F. Fischer, E. Guilminot, M. Chatenet, A. Rigacci, S. Berthon-Fabry, E. Chainet, P. Achard, Proceedings of Seventh European Symposium on Electrochemical Engineering, Toulouse, France, 2005.
[17] L. Geniès, R. Faure, R. Durand, Electrochim. Acta 44 (1998) 1317.
[18] S. Adora, Y. Soldo-Olivier, R. Faure, R. Durand, E. Dartyge, F. Baudelet, J. Phys. Chem. B 105 (2001) 10489.
[19] F. Rodriguez-Reinoso, M. Molina-Sabio, M.T. Gonzalez, Carbon 33 (1995) 15.
[20] A. Ahmadpour, D.D. Do, Carbon 34 (1996) 471.
[21] M. Molina-Sabio, M.T. Gonzalez, F. Rodriguez-Reinoso, A. Sepuldeva-Escribano, Carbon 34 (1996) 505.
[22] V. Gomez-Serrano, J. Pastor-Villegas, A. Perez-Florindo, C. Duran-Valle, C. Valenzuela-Calahorro, J. Anal. Appl. Pyrolysis 36 (1996) 71.
[23] V. Gomez-Serrano, F. Piriz-Almeida, C. Javier Duran-Valle, J. Pastor-Villegas, Carbon 37 (1999) 1517.
[24] A.C. Lua, J. Guo, Carbon 38 (2000) 1089.
[25] J. Kuhn, R. Brandt, H. Mehling, R. Petricevic, J. Fricke, J. Non-Cryst. Solids 225 (1998) 58.
[26] P.L. Antonucci, V. Alderucci, N. Giordano, D.L. Cocke, H. Kim, J. Appl. Electrochem. 24 (1994) 58.
[27] F. Rodriguez-Reinoso, Carbon 36 (1998) 159.
[28] M.C. Roman-Martinez, D. Cazorla-Amoros, A. Linares-Solano, C. Salinas-Martinez de Lecea, Curr. Top. Catal. 1 (1997) 17.
[29] C. Lin, J.A. Ritter, B.N. Popov, J. Electrochem. Soc. 146 (1999) 3639.
[30] K. Kinoshita, Carbon, Electrochemical and Physicochemical Properties, John Wiley & Sons, New York, 1988.
[31] F. Maillard, M. Eikerling, O.V. Cherstiuok, S. Schreier, E. Savinova, U. Stimming, Faraday Discuss. 125 (2004) 357.
[32] A.B. Bourlinos, D. Gournis, D. Petridis, T. Szabo, A. Szeri, I. Dekany, Langmuir 19 (2003) 6050.
[33] J. Hajek, P. Maki-Arvela, E. Toukoniitty, N. Kumar, T. Salmi, D.Yu. Murzin, J. Sol-Gel Sci. Technol. 30 (2004) 187.
[34] E. Theodoridou, A.D. Jannakoudakis, P.D. Jannakoudakis, N. Pagalos, J.O. Besenhard, C.I. Donner, M. Wicher, Electrochim. Acta 38 (1993) 793.
[35] O. Antoine, Y. Bultel, R. Durand, P. Ozil, Electrochim. Acta 43 (1998) 3681.
[36] J. Yamashita, T. Ojima, M. Shioya, H. Hatori, Y. Yamada, Carbon 41 (2003) 285.
[37] J.-T. Wang, R.F. Savinell, Electrochim. Acta 37 (1992) 2737.
[38] O. Antoine, R. Durand, J. Appl. Electrochem. 30 (2000) 839.